Materials Science and Engineering A 400–401 (2005) 166–169

MATERIALS SCIENCE & ENGINEERING A

www.elsevier.com/locate/msea

Dislocation dynamics simulations of fatigue of precipitation-hardened materials

C.S. Shin[a], M.C. Fivel[a,*], M. Verdier[b], C. Robertson[c]

[a] *Génie Physique et Mécanique des Matériaux, CNRS, Institut National Polytechnique de Grenoble, CNRS, BP 46, 38402 St. Martin d'Hères, France*

[b] *Laboratoire de Thermodynamique et Physico-chemie Metallurgiques, Institut National Polytechnique de Grenoble, CNRS, BP 75, 38402 St. Martin d'Hères, France*

[c] *Commissariat à l'Energie Atomique, SRMA Saclay, 91191 Gif-sur-Yvette, Paris, France*

Received in revised form 23 December 2004; accepted 3 January 2005

Abstract

Fatigue tests of precipitation-hardened material are simulated in 3D using a new parallel discrete dislocation dynamics code. Simple geometries are used for the simulation volume and the particles. The evolution of the particle's strength by shearing-off is assumed in a simplified manner in order to study the effects of shearable and non-shearable particles on the formation of the PSBs. The simulated microstructural features of fatigue are in good qualitative agreement with experimental observations. Dislocation mechanisms for PSBs formation are detailed in this work.

Keywords: Dislocations; Plastic deformation; Fatigue; Parallelization

1. Introduction

Multi-phase materials which contain precipitates often show a good static strength compared to single-phase materials. Under cyclic loading conditions, however, precipitation-hardened materials do not always insure better fatigue properties. A few of the characteristic fatigue properties observed in experiments (e.g. [1]) can be summarized as follows: in case of shearable particles, the cyclic strain becomes localized into persistent slip bands (PSBs) after an initial hardening stage. A drastic cyclic softening related to the destruction of the precipitation hardening in the PSBs leads to the early initiation of shear-type fatigue cracks at the PSBs surface intersection. In case of non-shearable particles, the cyclic softening is strongly reduced and the cyclic deformation behavior is much more stable.

The PSB formation and the early crack initiation have already been investigated in the case of 316L stainless steel ([2]) using the 3D discrete dislocation dynamics (DDD) method ([3]).

In this work, fatigue tests of precipitation-hardened materials are simulated in 3D using the same DDD model. The computational performance of the serial DDD code has been improved by parallelization so as to simulate dislocations interacting with thousands of precipitates. The effects of shearable and non-shearable particles on the formation of PSBs are studied, and dislocation mechanisms for PSBs formation are presented.

2. Simulation method

2.1. Geometries and materials parameters

A cylindrical grain geometry has been adopted for the shape of the simulated volume. The volume is assumed to be a surface grain of a fatigue tested specimen, i.e. the volume consists of one free surface whose normal vector is taken as [1 1 0] and grain boundaries which act as strong obstacles to

* Corresponding author. Tel.: +33 4 76 82 63 36; fax: +33 4 76 82 63 82.
E-mail address: marc.fivel@gpm2.inpg.fr (M.C. Fivel).

0921-5093/$ – see front matter © 2005 Elsevier B.V. All rights reserved.
doi:10.1016/j.msea.2005.01.079

dislocation motion. The diameter of the cylinder is 10 μm, its height is 5 μm. Image forces due to the free surface are not taken into account in this work.

The material's parameters used in this simulations are those of nickel ($G = 94.7$ GPa, $\nu = 0.276$, $b = 2.5$ Å).

Particles that are represented as facets with a pre-defined strength are randomly distributed in the cylindrical volume. Two cases of particle radius, $r_p = 160$ and 400 nm, are considered with the volume fraction v_f being fixed to 14% for all the cases. The particle's strength τ_{facet} is decreased linearly by $\tau_{facet}/(2r_p/b)$ with each event of dislocation passage through a given particle's facets (b is the magnitude of the Burgers vector). Particles of radius 160 nm are assumed to be easily shearable ($\tau_{facet}^{init} = 292$ MPa) and those of radius 400 nm are assumed to be non-shearable ($\tau_{facet}^{init} = 7310$ MPa). The image forces due to the elastic modulus difference are not computed and no stress fields around particles are considered for the simplification of computing.

Fatigue simulations are performed under a plastic strain control with a fully symmetrical push-pull loading ratio ($\epsilon_p^{max}/\epsilon_p^{min} = -1$), and an applied plastic strain amplitude $\Delta\epsilon_p = 1 \times 10^{-3}$. Details on loading conditions can be found in [2].

The initial dislocation microstructure in all the simulations is composed of four Frank-Read sources, in the form of pinned dislocation segments. All the Frank-Read sources are of the edge-type with the Burgers vector $a/2[1\bar{1}0]$ on the $(\bar{1}1\bar{1})$ slip plane. It should be noted that there is no dislocation nucleation around the particles and also that no dislocations are punched in from the free surface.

2.2. Parallel computing

The computing efficiency of the serial DDD code is improved by revisiting the 'box method' ([3]), and a speedup of 50 with errors lower than 3% is obtained in the typical situation of 20,000 segments submitted to tensile loading. Then a parallel DDD code [8] is developed over a distributed memory system using the standard Message Passing Interface. Attention is focused on the fact that the 3D array of boxes physically dividing the cubic simulation volume is similar to a matrix in the computer memory space. The cubic simulation volume is decomposed into parallel-piped subsystems which are mapped to processors. The boundaries of each parallel-piped system are dynamically moved to balance the computing load among the processors. Another speedup of around 17 is achieved when using 25 cpus to handle more than 30,000 segments.

3. Simulation results and discussion

The evolution of the total dislocation density, ρ_{tot} is monitored for the case $r_p = 160$ nm particles, $r_p = 400$ nm particles and no particles. ρ_{tot} is plotted as a function of the accumulated cyclic Von Mises strain in Fig. 1. The dislocation densities quickly increase and fluctuate according to the cyclic deformation in all the cases. Here saturation of the dislocation densities is not observed because of the relatively small number of fatigue cycles which have been performed (close to three cycles for $r_p = 160$ nm and five cycles for $r_p = 400$ nm). It is expected, however, that dislocation densities would gradually saturate as the fatigue cycles proceed as observed in [2].

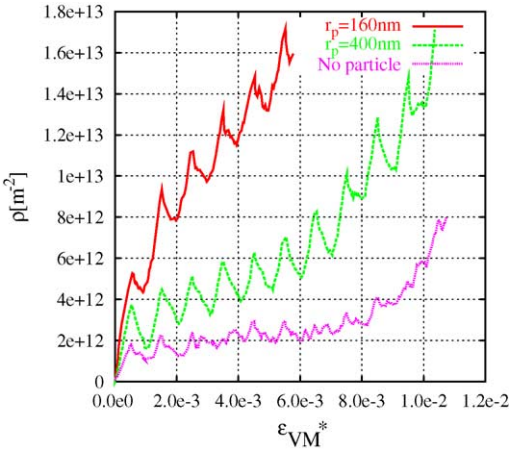

Fig. 1. Evolution of the total dislocation density of the volume containing particles with $r_p = 160$ nm, $r_p = 400$ nm and no particles.

Fig. 2 shows the dislocation microstructure formed after three cycles in the $r_p = 160$ nm particle case and after five cycles in the $r_p = 400$ nm case, along the [1 1 0] direction. The figures illustrate clearly that the dislocation structures are highly heterogenous and that intense slip bands are formed on the primary slip plane upon the cyclic loading.

Detailed observation of the dislocation microstructure reveals that the particles affect the slip localization in several ways:

(i) The width w_{disl} of the dislocation distributions over the simulation volume is the largest for $r_p = 400$ nm (non-shearable particles) and the smallest for $r_p = 160$ nm (shearable particles), i.e. $w_d^{r_p=400\,nm} > w_d^{No\ particle} > w_d^{r_p=160\,nm}$.

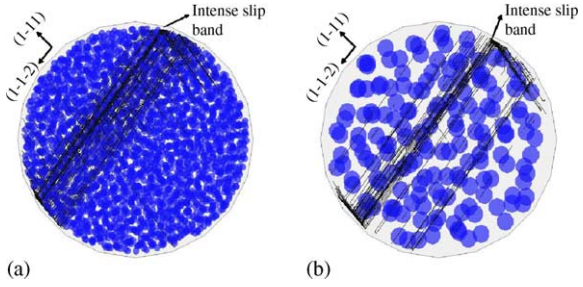

Fig. 2. Localization of slip by forming intense slip bands. (a) Particles with $r_p = 160$ nm and (b) particles with $r_p = 400$ nm.

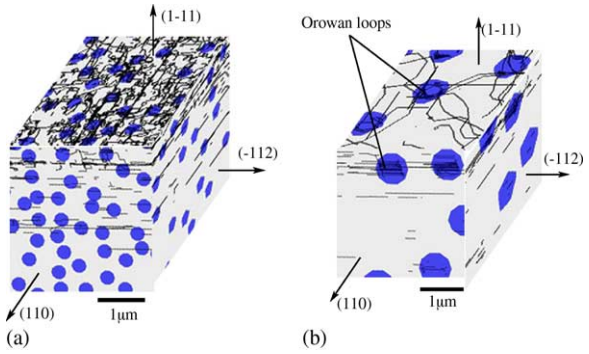

Fig. 3. 3D image of intense slip bands: (a) $r_p = 160$ nm; (b) $r_p = 400$ nm.

(ii) The maximum local dislocation densities (ρ_{max}) are in the following order, $\rho_{max}^{r_p=160\,nm} > \rho_{max}^{r_p=400\,nm} > \rho_{max}^{No\ particle}$.

(iii) The slip band width is smaller with shearable particles, i.e. $d_b^{r_p=400\,nm} > d_b^{r_p=160\,nm}$.

Item 1 demonstrates that non-shearable particles promote cross-slip due to the back stresses exerted by Orowan loops around the particles, and the dislocations easily sweep a large area of the simulation volume as a result. Items 2 and 3 are consistent with the experimental observations, according to which PSBs are much thinner if particles are shearable, and the local plastic strain becomes higher as the PSBs gets narrower ([5]).

Fig. 3(a) shows a 3D image of the dislocation structure viewed from the orientations normal to the $(1\,\bar{1}\,1)$ slip plane, $[1\,1\,0]$ (Burgers vector) and $[\bar{1}\,1\,2]$ at cycle number 3 with $\epsilon_p \sim 0$. In the plane normal to $[1\,1\,0]$, intense slip bands can be clearly seen in the form of thin and compact dislocation walls. In the plane normal to $[1\,\bar{1}\,1]$, the dislocation structure is quite heterogeneous, and shows ladder-like structures along the Burgers vector direction. Dislocation debris and small loops are also visible between the particles. It should be noted that the residual dislocation tangles are different in size compared to those in the single-phased material case, in which large tangles are observed together with ladder-like slip bands ([2,4]).

Fig. 3(b) shows the intense slip bands for non-shearable particle case ($r_p = 400$ nm) at cycle number 5 with $\epsilon_p = 0$. The wall thickness of the PSB is much larger than in the previous case, and the dislocation densities are varied in the band seen along the $[1\,1\,0]$ direction. In the $(1\,\bar{1}\,1)$ plane, several Orowan loops and dense dislocation tangles are formed around the particles. In the space between the particles, however, long dislocation lines are clearly visible.

4. Microstructure formation mechanisms

In the case of shearable particles ($r_p = 160$ nm), there is a limited number of easy glide paths for dislocations. Thus, slip bands would form along one of the easy glide paths whose thickness is usually limited (order of r_p). Upon load reversal, double cross-slipped dislocations glide in the opposite direction along path close to the initial glide path because (i) dislocations also have a limited free-flight distance in the cross-slip plane and (ii) the particles in the initial path loose part of their initial strength. This would form closely spaced edge dipoles, so called vein structures. As cycling proceeds, the subsequent cross-slipped screw dislocations due to the cyclic loading react with the edge dipoles and produce prismatic loops aligned in the Burgers direction or helicoidal structures as observed in single-phased materials ([6]) but with a much smaller size.

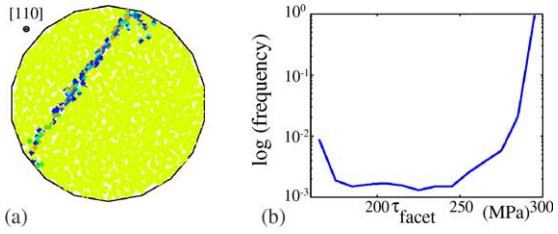

Fig. 4. Loss of the particle's strength in the case of shearable particles ($r_p = 160$ nm). (a) Spatial distribution of particle strength and (b) repartition by the particle strength.

The repeated motion of interfacial dislocations with the cycles will eventually make particles at the PSBs edges to loose their strength, and persistent bands will be formed at this place. This process is observed numerically in the simulations as shown in Fig. 4. A clear channel of sheared particles is visible and its position corresponds exactly to that of the intense slip band (see Fig. 4(a)). Fig. 4(b) shows the statistical distribution of the facet's residual strength after three cycles. The facet strengths are distributed as follows: most of the facets are not sheared and keep their initial strength (right peak) and a small portion of the facets is completely sheared (left peak).

In the case of non-shearable particles, accommodation of the applied plastic strain is much easier because dislocations can move over a relatively long distance on the glide plane. During the first few cycles, the particles are bypassed by the Orowan mechanism. Glissile loops are accumulated around the particles. When the critical stress is reached, the screw portions of the loops change their glide plane by cross slip, which contribute both to propagate slips in the simulation volume by generating dislocations in the secondary plane, and to the formation of 3D loops around the particles. Interactions between these loops and the dislocations in the secondary plane eventually form dense tangles around the particles. As the cyclic deformation proceeds, the tangles around the particles act as pinning points for dislocations moving between the particles. It thus favors the formation of dislocation dipoles which are linked by two near particles. The cutting of these dipoles by freely gliding dislocations then generate stable dislocation structures. The subsequent formation of dipoles

between the particles and the dislocation interactions produces dense dislocation structures between the particles. This mechanism explains the dense dislocation tangles observed around the particles and complex dislocation structures between pairs of closely spaced particles [7].

References

[1] V. Gerold, D. Steiner, Scrpita Metall. 16 (1982) 405–408.
[2] C. Déprés, M.C. Fivel, C.F. Robertson, Phil. Mag. 84 (22) (2004) 2257–2275.
[3] M. Verdier, M.C. Fivel, I. Groma, Model. Simul. Mater. Sci. Eng. 6 (1998) 755.
[4] K. Obrtlik, T. Kruml, J. Polák, Mater. Sci. Eng. A187 (1) (1994) 1–10.
[5] J.K. Lee, C. Laird, Phil. Mag. 47A (1983) 579–597.
[6] Y. Li, C. Laird, Mater. Sci. Eng. A186 (1–2) (1994) 65–86.
[7] C.S. Shin, PhD Thesis, GPM2/INP Grenoble, 2004.
[8] C.S. Shin, M.C. Fivel, M. Verdier, K.H. Oh, J. Comput. Phys.